Pure Appl. Chem., Vol. 74, No. 9, pp. 1707–1718, 2002.

Mesoscopic domains of cobalt nanocrystals*

M. P. Pileni

Université Pierre et Marie Curie, Laboratoire des Matériaux Mésoscopiques et Nanomètriques, LM2N, UMR CNRS 7070, 4 Place Jussieu, 75251 Paris Cedex, France

Abstract: In this paper, various mesoscopic structures made of cobalt nanocrystals are presented. It is demonstrated that the evaporation time and the application of an external magnetic field during the evaporation process play a major role in the shape of mesostructure obtained. Their magnetic properties change with the shape of the mesostructure.

INTRODUCTION

In recent years, ferromagnetic nanomaterials have received considerable attention, both theoretically and experimentally, owing to their potential in developing high-density magnetic recording media, and to their fascinating experimental behavior. The behavior of isolated magnetic nanoparticles has been extensively studied and is rather well understood [1]. In these dense systems, the mutual interactions, in particular the dipolar interactions, play an important role. These studies have been greatly extended, as the smaller magnetic particles become superparamagnetic at room temperature. This induces random fluctuations of the magnetic moment in the nanocrystals and then a limit in the storage density. On the other hand, when they are agglomerated in dense systems such as granular films, the magnetic properties largely differ both from those of the individual nanocrystals and the bulk materials [2].

There are numerous results for granular magnetic solids [1,2], but none for 3D superlattices. For nonmagnetic material, 3D "supra" crystals of nanoparticles are produced [3–7]. By controlling substrate temperature and evaporation rate, "supra" crystals made of more than a thousand layers of nanocrystals are obtained [6,7]. With magnetic nanocrystals, until now, it was impossible to produce "supra" crystals. However, very recently [8], in our laboratory, we have been able to make large "supra" crystals. This provides great hope and a fascinating new field of physical chemistry. These artificial structures can be manipulated to achieve tailored materials for application and for exploration of physical phenomena, as the magnetic properties of this new class of materials should, as with dense films, differ both from those of individual nanoparticles and bulk materials.

In our laboratory, collective magnetic properties have been demonstrated when cobalt nanocrystals are self-organized in a 2D hexagonal network. There is an increase in the blocking temperature, and the magnetization curve, when measured with an applied field parallel to the surface, is squarer than that of the same nanocrystals isolated in liquid solution [9,10]. This behavior is explained in terms of dipolar interactions between adjacent nanocrystals in the self-organized monolayer [11]. The organization induced by an applied magnetic field enables fabricating 3D superlattices of ferrite nanocrystals [12,13]. Collective magnetic properties due to partial orientation of easy magnetic axes during the deposition were reported [13].

Pure Appl. Chem.* **74, 1489–1783 (2002). An issue of reviews and research papers based on lectures presented at the 2nd IUPAC Workshop on Advanced Materials (WAM II), Bangalore, India, 13–16 February 2002, on the theme of nanostructured advanced materials.

SYNTHESIS OF COBALT NANOCRYSTALS

Cobalt nanocrystals [9,14] are produced by using reverse micelles made of cobalt 2-ethylhexyl sulfosuccinate, usually called $Co(AOT)_2$, ($[Co(AOT)_2] = 0.125$ M). The water content, defined as $w = [H_2O]/[AOT]$, is fixed at 35, and $Co(AOT)_2$ is reduced by using sodium tetrahydroboride, $NaBH_4$, (2×10^{-2} M). Immediately after borohydride addition, the color of the micellar solution turns from pink to black, indicating the formation of particles. Addition of lauric acid, $C_{12}H_{25}COOH$, to the micellar solution induces an attachment with cobalt atoms located at the interface. The coated cobalt nanocrystals are extracted from reverse micelles by ethanol addition. The particles are then washed and centrifuged several times with ethanol to remove all the surfactant. A black powder is obtained. This chemical surface treatment highly improves the stability of cobalt exposed to air, and cobalt nanocrystals can thus be stored without aggregation. The powder is analyzed by the extended X-ray absorption fine structure (EXAFS) technique and compared to a reference of pure cobalt metal. The best fitting of the EXAFS spectrum for nanocrystal powder [15] is obtained by assuming a core of cobalt metal with an interatomic $R_{Co\text{-}Co} = 2.5$ Å. It is characteristic of the metallic behavior of the cobalt nanoparticles and a surface shell, where Co atoms are linked to light elements such as oxygen with a distance $R_{Co\text{-}O} = 2$ Å. The presence of oxygen at the surface is due to the coating of the nanocrystals by lauric acid, $C_{12}H_{25}COOH$. Of course, a cobalt oxide layer surrounding the cobalt core cannot be excluded. From these, it is concluded that there is formation of cobalt metal nanoparticles. The average diameter of these nanoparticles, determined by transmission electron microscopy (TEM), is 8.0 nm (Fig. 1) with a polydispersity of 14 %.

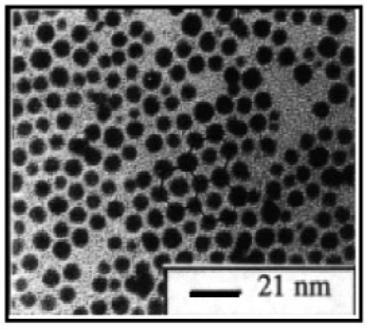

Fig. 1 TEM image of cobalt nanocrystals.

MESOSCOPIC STRUCTURES MADE OF 8-nm COBALT NANOCRYSTALS

To grow 3D superlattices of cobalt nanocrystals, the evaporation rate has to be very low. Freshly cleaved HOPG substrate is immersed a solution composed of cobalt nanocrystals dispersed in hexane. The evaporation occurs under air or hexane vapor and produces a black magnetic film. The evaporation time is 45 min under air and 12 h under hexane vapor.

Mesoscopic structures obtained in absence of external forces [16]

Without any applied magnetic field during the deposition process, the scanning electron microscopy (SEM) images differ with the deposition conditions. For evaporation under air, the SEM pattern is that of a homogeneous film (Fig. 2A). Magnification of this image shows that it is highly porous (Fig. 2B) and made of spherical aggregates with an average diameter of 70 nm (Fig. 2C). It must be pointed out that these 70-nm aggregates consist of 8-nm coated cobalt nanocrystals.

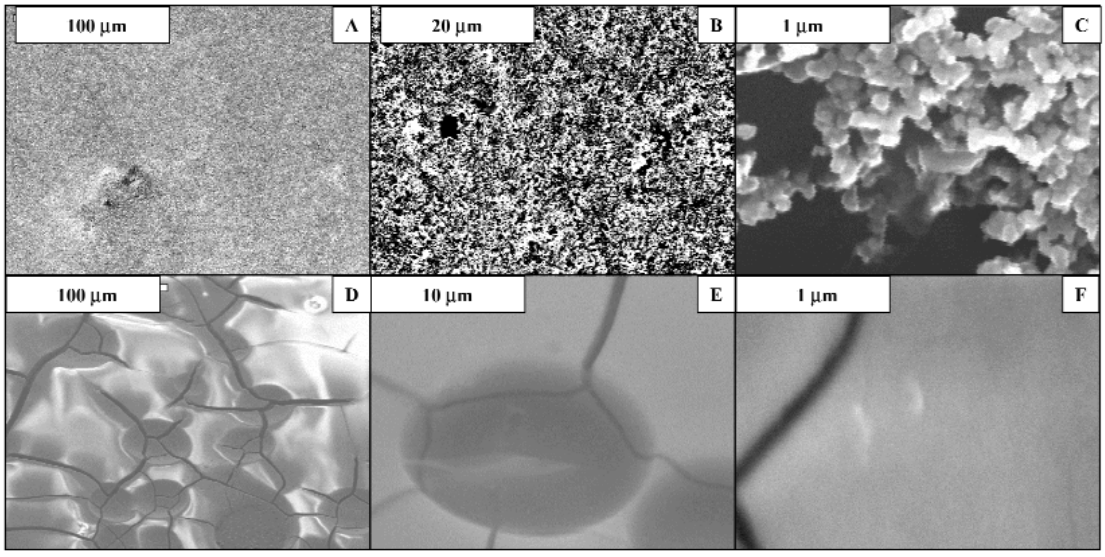

Fig. 2 SEM patterns at different magnifications of the film, deposited without a magnetic field, obtained by evaporating a solution of cobalt nanocrystals on HOPG substrate. A, B, C: The evaporation time under air is 45 min. D, E, F: The evaporation time under hexane is 12 h.

A change in the film behavior is observed when the evaporation occurs under hexane vapor. The film is more homogeneous and smoother (Fig. 2D) than that observed under air (Fig. 2A). However, numerous discontinuities are present. There is a large domain formed by the stacking of several layers of nanocrystals, and holes are observed on the film (black spot on the SEM patterns). The height of the film is around 2 µm (Fig. 2E). The internal structure of the film appears homogeneous (Figs. 2E and 2F) without any spherical aggregates as observed after evaporation under air (Fig. 2C). X-ray reflectivity measurements show one large peak at 0.07 $Å^{-1}$ corresponding to an average characteristic distance between two nanocrystals of 9 nm. This is close to that observed by TEM in 2D monolayers [15]. The lack of peaks at high q values indicates the absence of long-distance order in the film. From these data, it is concluded that the film obtained when the evaporation is performed under hexane vapor is more homogeneous, but there is no long-distance order.

These changes in morphology with evaporation under either air or hexane vapor are related to the evaporation rate. Under hexane vapor atmosphere, the nanocrystals freely diffuse in solution leading to the formation of homogeneous structures. Hence, the observed film is made of aggregates, without a defined shape, dispersed or agglomerated on the substrate. No 3D "supra" crystals are observed. However, by changing the experimental conditions, the produced cobalt nanocrystals self-organize in well-ordered 3D superlattices [8].

Mesoscopic structures obtained by applying a magnetic field perpendicular to the substrate [17]

An external magnetic field perpendicular to the substrate is applied during the deposition process. It is expected that each nanocrystal moment is aligned in the field direction. Figure 3 shows a large variety of mesoscopic structures of cobalt nanocrystals with various shapes, which depend on the field strength. As shown above with no applied field, a large-scale SEM picture shows a very inhomogeneous and amorphous structure (Fig. 3A). At a very low applied field (H = 0.01 T), there are large dots as shown

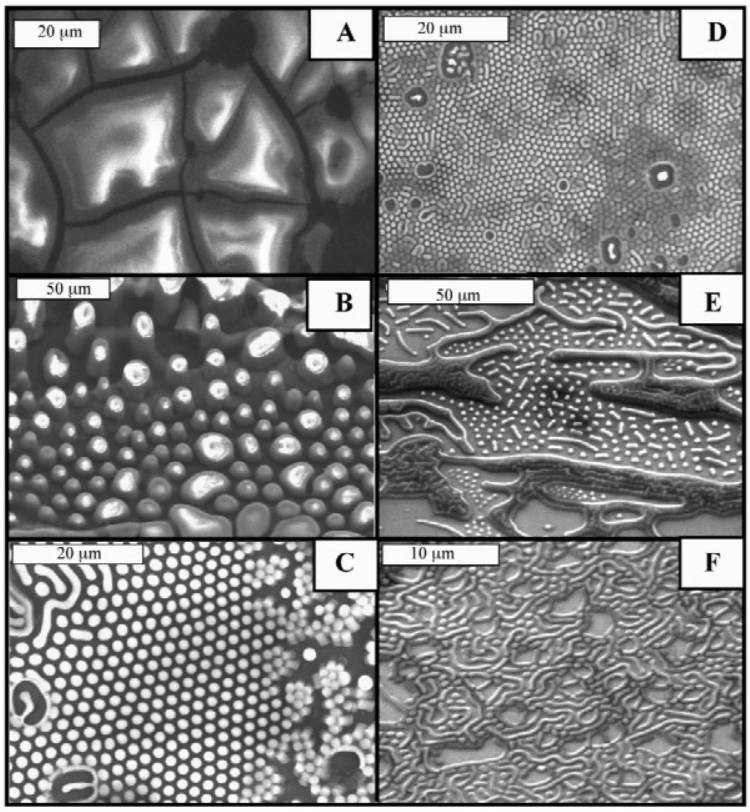

Fig. 3 SEM patterns obtained by evaporating a concentrated solution of cobalt nanocrystals deposited under a magnetic field perpendicular to the HOPG substrate. The evaporation time is 12 h. The strength of the applied field is 0 (A); 0.01 T (B); 0.27 T (C); 0.45 T (D); 0.60 T (E); and 0.78 T (F).

in Fig. 3B with a rather wide size distribution. On increasing the applied magnetic field to 0.27 T, well-dispersed dots are observed (Fig. 3C). A further increase in the applied field to 0.45 T shows patterns similar to those seen under 0.27 T (Fig. 3C). However, the average diameter and inter-dot distance are markedly reduced. More quantitative data can be derived from enhancement of the various structures (Fig. 4). At a low applied field (0.01 T), the size, inter-dot distance (core to core), and the size distribution of the dots are rather large (see Fig. 4A and Table 1). The increase in the applied magnetic field strength induces formation of well-defined columns with a very sharp interface (Fig. 4B) and also results in a drastic decrease in the height of these columns (Table 1). A further increase in the applied field (Fig. 4C) induces a marked decrease in the diameter of dots, the inter-dot distance, and in the height. The size distribution of dots slightly increases compared to that observed when the applied field is 0.27 T. Hence, for a given applied field, the size and inter-dot distance are rather low. On increasing the applied field, the diameter, the height, and the distance between dots decreases. The latter evolves continuously with the reciprocal of the applied magnetic field. By applying a magnetic field of 0.60 T, drastic changes are observed. Figure 3E shows the presence of dots, worm-like and labyrinth-like structures. A further increase in the magnetic field to 0.78 T enables formation of a homogeneous labyrinth structure.

From these data, it is concluded that by applying a magnetic field during the cobalt nanocrystal deposition on a substrate, it is possible to form well-defined 3D superlattices. The structure is observed on a very large scale (up to 0.02 mm^2). Addition of a hexane drop to the substrate totally destroys these

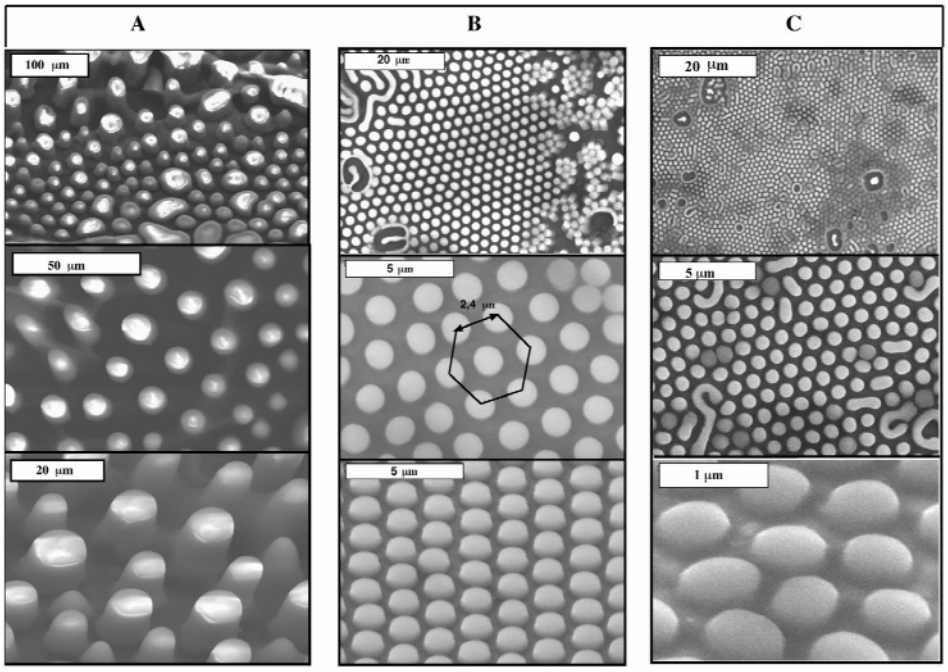

Fig. 4 SEM patterns at different magnifications of superlattices obtained on HOPG substrates, with an applied field of 0.01 T (A), 0.27 T (B), and 0.45 T (C). The tilted SEM patterns showing the 3D structures and height of the dot are deduced for each pillar.

Table 1 H, Do, Di, σ, and h are the strength of the applied field, the dots diameter, the inter-dots distance, the size distribution and the height of the dots, respectively.

H (T)	Do (µm)	Di (µm)	σ (%)	h (µm)
0.01	11.7	14.3	25	8
0.27	1.7	2.4	5%	0.5
0.45	0.75	1.1	10	0.3

structures, and cobalt nanocrystals are dispersed in the solvent. The TEM images for these collected nanocrystals remain the same as that observed in Figure 1, indicating that no coalescence takes place when nanocrystals form a 3D film. Whatever the superlattices are, the background of the sample is covered by multilayers made of cobalt nanocrystals. The superlattices sit on the film having an average height of a few µm. Similar patterns were observed previously [18–22]. When a magnetic fluid is confined with an immiscible nonmagnetic liquid between closely spaced horizontal glass plates (Hele–Schaw cell) and subjected to an external magnetic field perpendicular to the plate, labyrinths and hexagonal arrays of columns are formed [19,23–29]. These patterns are produced at the interface between the magnetic and nonmagnetic phases, and they are explained in terms of competition between the magnetic and surface energy. The surface tension tends to minimize the area of the interface, whereas the interactions between magnetic dipoles favor its extension. The size of the patterns is determined by minimizing the free energy [30,31]. The influence of the method for computing the magnetic energy has been studied. The ratio of the magnetic to the nonmagnetic liquid is an important factor for the relative stability of the patterns.

More quantitative data are deduced by using the same parameters developed by Flores et al. [32] for magnetic fluids. These parameters are:

- The parameter e is the ratio of the end-to-end length to width. If $e > 2$, the superlattice is classified as worm-like. If $e = 1$, it is called dots, and if $1 < e < 2$, it is disk-like.
- P is the ratio of the number of worms to the total number of aggregates:

  $P = N_{e \geq 2} / N_{\text{total}}$
- C is given by the perimeter of (aggregates) / $2\sqrt{(\pi}$ area of aggregates). Thus, the average complexity is :

  $\langle C \rangle = \sum C_i / N_{\text{total}}$

Figure 5 shows that the superlattice evolves from disk-like to columns and then to worms. The data presented above show three behaviors:

- Under a very low perpendicular applied field ($H \leq 0.01$ T), a transition from agglomerated cobalt nanocrystals to disk-like structures with a rather large size, shape, and inter-dot distance distribution takes place.
- In the $0.01 \text{ T} < B < 0.47$ T range, well-defined hexagonal patterns are observed.
- At 0.47 T, the transition onset from columns, well dispersed in a hexagonal network, to worms and labyrinths is observed. At and above 0.78 T, well-defined labyrinths are seen, and they are probably due to fusion of dots (Fig. 6).

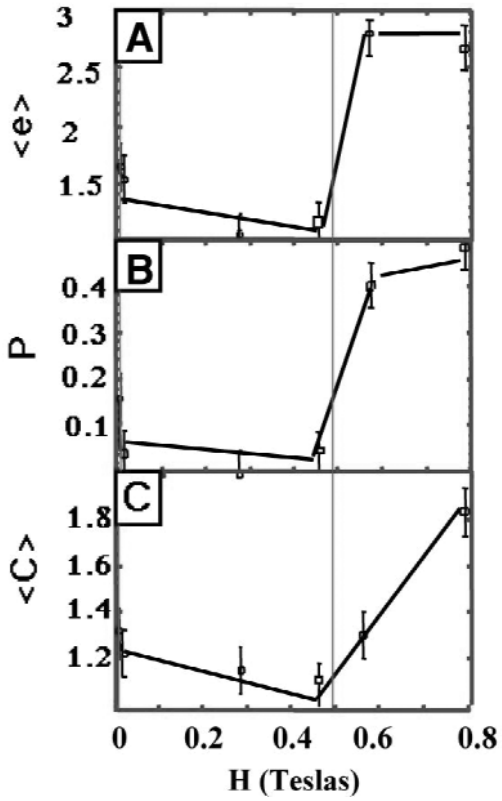

Fig. 5 Variation of the average form factor <*e*> (A); the worm ratio, *P* (B); the average complexity <*C*> with the intensity of the applied field during the deposition of the cobalt nanoparticles on the substrates.

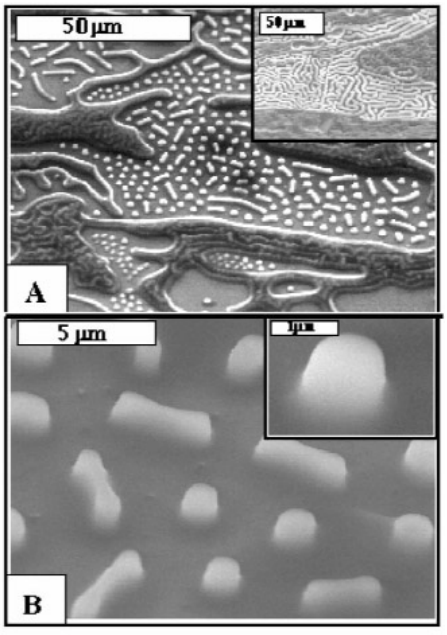

Fig. 6 SEM patterns at different magnifications of superlattices obtained on HOPG substrates, with an applied field of 0.56 T. The tilted SEM pattern shows the 3D structures.

Mesoscopic structures of cobalt nanocrystals obtained by applying a magnetic field parallel to the substrate [16]

Shape of mesoscopic structures

When a 0.78 T magnetic field is applied during evaporation under air, linear structures of cobalt nanocrystals, aligned along the applied magnetic field direction, are observed (Figs. 7A–7C). The increase in the magnification shows that the film is still highly porous (Fig. 7C) and is made of 70-nm spherical aggregates, as observed in the absence of a magnetic field (Fig. 2C). Hence, at high magnification, no differences in the SEM patterns obtained in the absence (Fig. 2C) and in the presence (Fig. 7C) of a magnetic field are observed, indicating that the organization takes place at the macroscopic level. When the evaporation occurs under hexane vapor, at a fixed applied magnetic field (0.78 T), the structure of the film drastically changes (Figs. 7D, 7E, and 7F). Long stripes in the direction of the applied field without any holes and cracks are formed. Magnification of the stripes shows a highly compact film (Figs. 7E and 7F) with 2 µm average film height. From these data, it can be concluded that evaporation in a high applied magnetic field leads to the formation of mesoscopic scale structures of nanocrystals aligned along the field direction.

Similar behavior to that described above under hexane evaporation is observed at various applied fields. Figure 8 shows that, for any applied field, stripes are formed with a periodic structure. The roughness and the average distance between two adjacent stripes vary. A characteristic wavelength, λ_χ, is defined as the average distance between two adjacent stripes. With increasing the strength of the applied field, this distance decreases to reach a plateau around 0.56 T (Fig. 9). Simultaneously, the stripes are sharper. The order and compacity of stripes increases with increasing the applied field [12,13]. Similar behavior was observed by applying a parallel field in a Hele–Shaw cell, with organization of magnetic fluids in stripes. The process takes place in two steps [18,33,19]:

- Formation of single chains or small linear aggregates is rapid and occurs in a few minutes.
- On a longer time scale, in order to minimize the magnetic energy, the chains clump together to form regular stripe patterns. This dynamic process takes place in one or two hours, depending on the materials and on the thickness of the cell. The differences in the stripe organization (Fig. 7) observed under air and hexane vapor are related again to the evaporation rate: with fast evaporation (under air), chains are formed on a macroscopic scale. With slow evaporation, the two processes described in a magnetic fluid occur with formation of parallel stripes and local homogeneous structures. However, a major difference can be noticed in the nature of the patterns: conversely to the ferrofluids, the array of cobalt nanocrystals persists after the field is switched off.

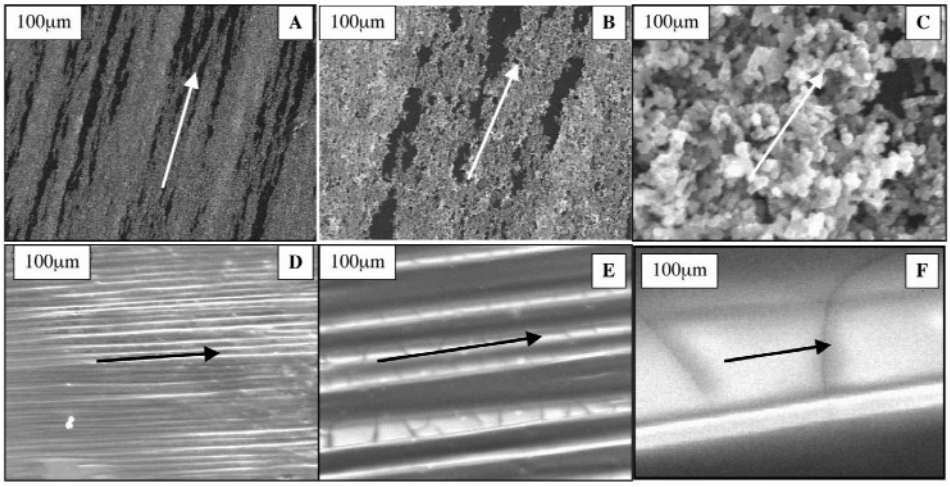

Fig. 7 SEM patterns at different magnifications of the film, deposited with a magnetic field parallel to the substrate, obtained by evaporating a solution of cobalt nanocrystals on HOPG substrate. A, B, C: The evaporation time under air is 45 min. D, E, F: The evaporation time under hexane is 12 h.

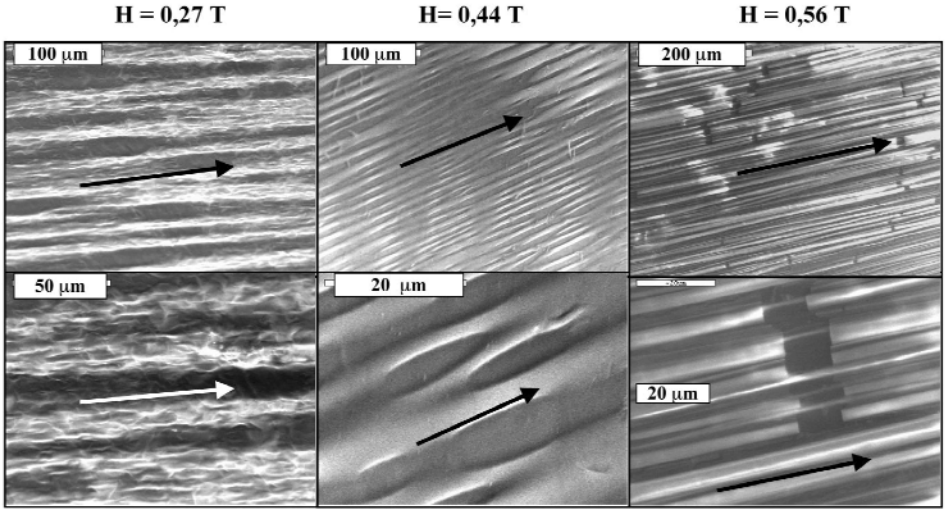

Fig. 8 SEM patterns, and one tilted at 45°, of the film obtained in various magnetic fields by evaporating a solution of cobalt nanocrystals on HOPG substrate.

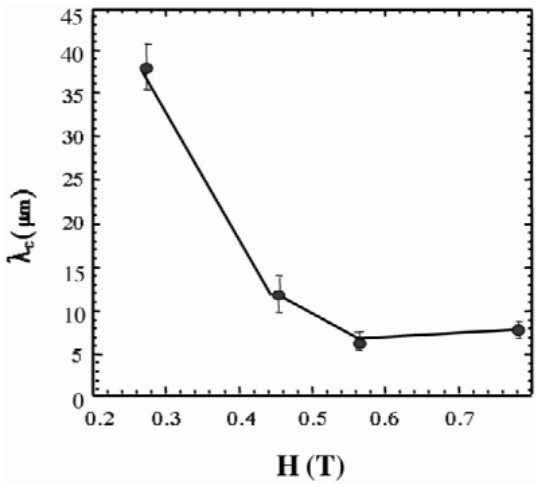

Fig. 9 Variation of the critical wavelength, λ_χ, (distance center to center between two adjacent stripes) with the intensity of the field applied during the evaporation process.

MAGNETIC PROPERTIES [16]

The magnetic properties of the compact 3D organization in stripes, shown in Fig. 8, are recorded. For simplicity, the samples obtained by applying 0.01, 0.27, 0.45, 0.56, and 0.78 T fields are called A, B, C, D, E, respectively. The hysteresis loops are recorded at 3 K when the applied magnetic field is parallel to the substrate and to the direction of the stripes. Under these experimental conditions, the nanocrystals form a thin film, and the demagnetizing factor is close to zero for each sample. Figure 10 shows a change in the hysteresis loop with the various samples. The hysteresis loop of A is inside that of B. Similarly it is squarer for C than B, for D than for C. The higher the deposition field, the squarer is the hysteresis loop. At the highest deposition field value (sample E, H = 0.78 T), a slight decrease in the hysteresis squareness is observed. This increase in the reduced remanence with increasing the applied field can be due either to orientation of the easy axes during the evaporation process, as already observed with maghemite nanocrystals [13], or to formation of ferromagnetic domains induced by dipolar interactions. To differentiate between these two phenomena a model is developed.

The magnetization curves are numerically calculated for an assembly of noninteracting particles with cubic anisotropy. Two possibilities, namely, $K > 0$, where the particles have 3 easy axes and $K < 0$ where the particles have 4 easy axes ([111] directions) are considered. With cubic anisotropy totally oriented in the field $\boldsymbol{H}_d$, the reduced remanence is $M_r/M_s \approx 0.90$ and $M_r/M_s = 1.00$, for $\boldsymbol{H}_m$ normal and parallel to $\boldsymbol{H}_d$, respectively. In the case of a random distribution of the easy axes, one has $M_r/M_s = 0.832$ if $K > 0$ and $M_r/M_s = 0.866$ if $K < 0$ [34]. This small variation shows that it is nearly impossible to ascertain if the easy axes of cobalt nanocrystals are oriented only from the knowledge of $M(H_m^{//})$ and $M(H_m^{\perp})$. Due to this, it is impossible reach a conclusion concerning the orientation of the easy axes for cubic anisotropy nanocrystals from the comparison of the magnetization curves $M(H_m^{//})$ and $M(H_m^{\perp})$. This is confirmed experimentally. Figure 11 shows the magnetization hysteresis loops recorded when the applied field is parallel and perpendicular to the stripes. The two curves are more or less superimposed, and there are no significant differences between them. However, the increase in the reduced remanence with increasing the magnetic field applied during the deposition cannot be neglected. This can be related to the decrease in the characteristic distance of the stripes. It decreases with increasing the applied magnetic field during the evaporation process. This is confirmed by the fact that the reduced remanence increases linearly with the reciprocal of the characteristic distance (Fig. 12). This could be explained by:

- The surface anisotropy is predominant compared to the magneto-crystalline one. This has been demonstrated with cobalt clusters (3–4-nm diameter) fabricated by the low-energy cluster beam deposition technique [35].
- These nanocrystals embedded in the niobium film are characterized by a cubic anisotropy. Magnetization of an individual cluster (3-nm) provides the main contribution to magnetic anisotropy [36]. Hence, the cubic magneto-crystalline anisotropy is negligible compared to the surface anisotropy due to the symmetry breaking and surface strains.
- Because of the long alkyl chain used as coating, van der Wals interactions between objects increase during the evaporation process. This has been well demonstrated with reverse micelles [37]. Under an applied field, dipole–dipole interactions are added to the previous one. Such interactions increase with the strength of the applied field. Hence, in solution, aggregates made of isolated nanocrystals, at a fixed distance from each other, can be formed. The size of such aggregates increases with the strength of the applied field. At the end of the evaporation process, the field is formed by aggregates composed of isolated nanocrystals, inducing formation of ferromagnetic domains. Simulations developed previously for nanocrystals organized in 2D on hexagonal networks having a large coupling constant indicate formation of a ferromagnetic domain induced by dipole–dipole interactions [38]. In a previous paper [11], it is shown that cobalt nanocrystals are characterized by a low coupling constant (α_d = 0.05), whereas such ferromagnetic domains appear at zero field for a coupling constant greater than 0.2. However, the simulations were done at zero field for a 2D superlattice organized in a hexagonal network and not for a 3D film composed of several layers of cobalt nanocrystals deposited in a field. Thus, both the effect of dipolar interactions between adjacent nanocrystals and a partial alignment of the easy axes could explain the increase in the reduced remanence with increasing the applied magnetic field during the deposition with appearance of collective properties due to organization of cobalt nanocrystals are observed.

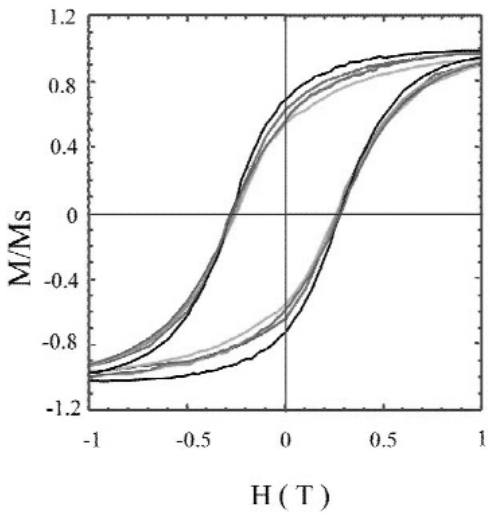

Fig. 10 Hysteresis curves measured at 3 K of samples obtained by applying a magnetic field during the deposition process: 0.01, 0.27, 0.45, 0.56, and 0.78 T.

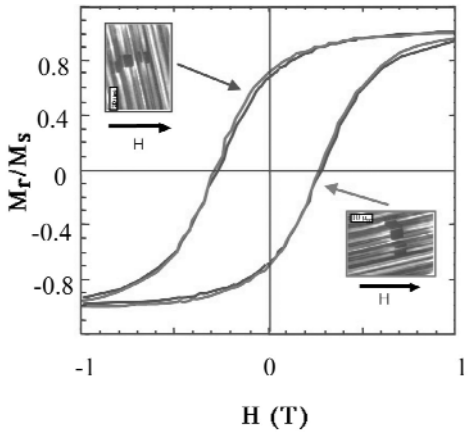

Fig. 11 Hysteresis curves obtained at 3 K for samples D (obtained) at 0.56 T. The measurement field is either parallel (light gray) or perpendicular (black) to the stripes. The substrate is kept parallel to the measurement field.

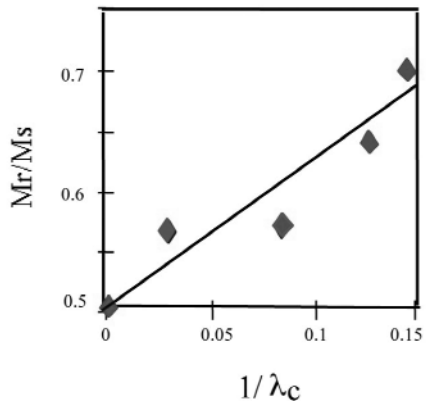

Fig. 12 Variation of the reduced remanence of the 3D arrays of cobalt nanocrystals with the reciprocal of the critical wavelength, λ_{χ}. The solid line is a visual guide.

CONCLUSION

In this paper, it is demonstrated that cobalt nanocrystals are organized in 3D superlattices. However, to obtain such patterns, it is necessary to apply a magnetic field during the evaporation process in order to overcome the magnetic frustration of the 2D superlattices. Thus, depending on the intensity of the applied field, various structures are obtained, such as unorganized dots, hexagonal networks of magnetic pillars, or a labyrinth. This is the first evidence of the formation of dense hexagonal patterns of magnetic dots made with cobalt nanocrystals obtained by wet chemistry. Such a new class of magnetic materials could offer numerous applications both in applied and theoretical physics, particularly for studying the collective magnetic properties in 3D supra organization of magnetic nanocrystals.

The magnetic properties of the superlattices show collective behavior related to the dipolar interactions between adjacent nanocrystals in the 3D structure and/or to the orientation of the magnetic moment of the particles during the deposition process in a magnetic field. However, due to the cubic anisotropy of cobalt nanocrystals, it is not possible at this stage to ascertain if the order has a strong influence on the magnetic properties of the magnetic film.

ACKNOWLEDGMENTS

The author would particularly like to thank Dr. J. Legrand who did most of the work. Thanks are also due to Drs. C. Petit, D. Ingert, J. Richardi, and V. Russier.

REFERENCES

1. J. L. Dorman, D. Fiorani, E. Tronc. *Advances in Chem. Physics*, Vol. XVIII, I. Prigogine and S. A. Rice (Eds.), p. 283, Wiley, New York (1997).
2. C. L. J. Chien. *Appl. Phys*. **69**, 5267 (1991).
3. L. Motte, F. Billoudet, M. P. Pileni. **99**, 16425 (1995).
4. L. Motte, F. Billoudet, E. Lacaze, M. P. Pileni. *Adv. Mater*. **8**, 1018 (1996).
5. A. Taleb, C. Petit, M. P. Pileni. *Chem. Mater.* **9**, 950 (1997).
6. A. Courty, C. Fermon, M. P. Pileni. *Adv. Mater*. **13**, 254 (2001).
7. A. Courty, O. Araspin, C. Fermon, M. P. Pileni. *Langmuir* **17**, 1372 (2001).
8. I. Lisiecki and M. P. Pileni. Unpublished data.
9. C. Petit, A. Taleb, M. P. Pileni. *Adv. Mater*. **10**, 259 (1998).
10. C. Petit, A. Taleb, M. P. Pileni. *J. Phys. Chem. B* **103**, 1805 (1999).
11. V. Russier, C. Petit, J. Legrand, M. P. Pileni. *Phys. Rev. B* **62**, 3910 (2000).
12. A. Ngo and M. P. Pileni. *Adv. Mater*. **12**, 276 (2000).
13. A. Ngo and M. P. Pileni. *J. Phys. Chem. B* **105**, 53 (2001); C. Petit, A. Taleb, M. P. Pileni. *J. Phys. Chem. B* **103**, 1805 (1999).
15. J. Legrand, C. Petit, D. Bazin, M. P. Pileni. *Appl. Surf. Sci*. **164**, 186 (2000).
16. C. Petit, J. Legrand, V. Russier, M. P. Pileni. *J. Appl. Phys*. **91**, 1502 (2002).
17. J. Legrand, A. Ngo, C. Petit, M. P. Pileni. *Adv. Mater*. **13**, 58 (2001).
18. M. Seul and D. Andelman. *Science* **267**, 476 (1995).
19. C. Y. Hong, I. J. Jang, H. E. Horng, C. J. Hsu, Y. D. Yao, H. C. Yang. *J. Appl. Phys*. **81**, 4275 (1997).
20. M. Ivey, J. Liu, Y. Zhu, S. Cutillas. *Phys. Rev. E* **63**, 11403 (2000).
21. S. Chizakumi. *The Physics of Magnetism*, Wiley, New York (1964).
22. H. Schmidt and R. J. Ram. *J. Appl. Phys.* **89**, 507 (2001).
23. L. T. Romanikew, M. M. G. Slusarczyk, D. A. Thompson. *IEEE Trans. Magn*. **11**, 25 (1975).
24. R. E. Rosensweig. *Ferrohydrodynamics*, Dover Publications (1986).
25. R. E. Rosensweig, M. Zahn, R. Shumovich. *J. Magn. Magn. Mater*. **39**, 127 (1983).
26. F. Elias, C. Flament, J.-C. Bacri, S. Neveu. *J. Phys. I (France)* **7**, 711 (1997).
27. J.-C. Bacri, R. Perzynski, D. Salin. *Endeavour, New Series* **12**, 76 (1988).
28. C.-Y. Hong, I. J. Jang, H. E. Horng, C. J. Hsu, Y. D. Yao, H. C. Yang. *J. Appl. Phys*. **81**, 4275 (1997).
29. C.-Y. Hong, C.-H. Lin, C.-H. Chen, Y. P. Chiu, S. Y. Yang, H. E. Horng, H. C. Yang. *J. Magn. Magn. Mater*. **226**, 1881 (2001).
30. J. Richardi, D. Ingert, M. P. Pileni. *J. Phys. Chem*. **106**, 1521 (2002).
31. J. Richardi, D. Ingert, M. P. Pileni. *Phys. Rev. E* (2002). In press.
32. G. A. Flores, J. Liu, M. Mohebi, N. Jamasbi. *Int. J. Mod. Phys. B* **13**, 2093 (1999).
33. R. Kaiser and G. Miskolczy. *J. Appl. Phys*. **41**, 1064 (1970).
34. C. G. Granquist and R. A. Buhrmann. *J. Appl. Phys.* **47**, 2200 (1976).
35. J. Tuaillon, V. Dupuis, P. Mélinon, B. Prevel, M. Treilleux, A. Perez, M. Pellarin, J. L. Vialle, M. Broyer. *Philosos. Magn. A* **76**, 493 (1997).
36. M. Jamet, W. Wernsdorfer, C. Thirion, D. Mailly, V. Dupuis, P. Melinon, A. Perez. *Phys. Rev. Lett*. **86**, 4676 (2001).
37. G Cassin, J. P. Badiali, M. P. Pileni. *J. Chem. Phys*. **99**, 12941 (1995).
38. V. Russier. *J. Appl. Phys*. **89**, 1287 (2001).